

Submonolayer molecular hydrogen on graphite: A path-integral Monte Carlo study

Kwangsik Nho and Efstratios Manousakis

Department of Physics and MARTECH, Florida State University, Tallahassee, Florida 32306

(Received 12 July 2001; revised manuscript received 3 October 2001; published 22 February 2002)

We have used path-integral Monte Carlo (PIMC) to simulate molecular hydrogen on graphite at submonolayer coverage. First we use a flat substrate and we study the first layer for various values of the coverage up to layer completion. We found that the first layer has a solid-gas coexistence phase at low densities and a triangular solid phase at and above the equilibrium density $\rho_0 = 0.0705 \text{ \AA}^{-2}$. We also determine that the first layer promotion coverage is at 0.094 \AA^{-2} in agreement with experiment. Second we introduce the full H_2 -graphite interaction, i.e., we include the effects of substrate corrugations. In this case we carry our PIMC simulations on a variety of systems at and below the $1/3$ coverage. We calculate the energy as a function of coverage, contour plots of the molecule probability distribution, the pair distribution function, the static structure function and the specific heat. When the substrate corrugation part of the interaction is included we find that at $1/3$ coverage the system is in a $\sqrt{3} \times \sqrt{3}$ commensurate solid phase. At coverages below that and at low enough temperature the system exists in solid clusters surrounded by vapor. At coverages below a critical density, defining a tricritical point, as the system is heated up these clusters melt into a uniform fluid phase. We find that below the commensurate density and above the tricritical point, as the clusters are heated up, first they undergo a transition into a phase where the vapor phase disappears and a commensurate phase with vacancies arises. This commensurate solid melts at higher temperature into a uniform fluid phase.

DOI: 10.1103/PhysRevB.65.115409

PACS number(s): 64.60.Fr, 67.70.+n

I. INTRODUCTION

Molecular hydrogen films adsorbed on the basal plane surface of graphite display formation of well-defined layers.¹⁻⁶ The phase diagram and the structure of the monolayer have been investigated by a number of experimental techniques, including heat capacity,¹⁻⁶ neutron scattering,⁷⁻¹⁸ nuclear magnetic resonance,¹⁹ and low-energy electron diffraction.^{20,21}

Similarly to helium physisorbed on graphite, submonolayer of molecular hydrogen adsorbed on graphite forms a $\sqrt{3} \times \sqrt{3}$ commensurate structure due to the graphite surface potential corrugation. When this structure is formed at areal density of $\rho_c = 0.0636 \text{ \AA}^{-2}$, the hydrogen molecules occupy one-third of all the graphite adsorption sites. The diffraction pattern shows a sharp Bragg peak at the position of $k = 1.703 \text{ \AA}^{-1}$. The phase diagram of molecular hydrogen on graphite at and below the $1/3$ coverage (where it forms the perfect $\sqrt{3} \times \sqrt{3}$ commensurate structure) is shown in Fig. 1. At densities below the commensurate density ρ_c the sharp Bragg peak remains at the same position. The low temperature low density (lower than $\sim 0.65\rho_c$) phase is composed of $\sqrt{3} \times \sqrt{3}$ commensurate solid clusters surrounded by vapor; thus, this phase contains the commensurate structure giving rise to the same Bragg reflection. This phase coexistence is also supported by the fact that the heat capacity isotherms vary linearly with coverage. As the temperature increases, the $\sqrt{3} \times \sqrt{3}$ commensurate solid phase melts into a two-dimensional (2D) fluid phase. The melting temperature can be determined from the specific-heat single peak. At coverages above $\sim 0.65\rho_c$ and up to ρ_c the specific heat shows two anomalies. First above a certain temperature of order 10 K, the vapor-phase component disappears and a uniform $\sqrt{3} \times \sqrt{3}$ commensurate solid phase with vacancies covers the

entire surface. In this coverage range the second specific heat peak, which appears at higher temperature, is due to the melting of this uniform commensurate solid. This is the order-disorder transition of the $\sqrt{3} \times \sqrt{3}$ commensurate phase. In the immediate neighborhood of ρ_c a value of the specific heat critical exponents α of 0.33 ± 0.03 is obtained.⁵ This value is in excellent agreement with the theoretical three-state Potts model value of $\alpha = 1/3$ (Refs. 22-25) as in the case of the helium isotopes.²⁶ This phase transition and the tricritical point belong to the universality class of the three-state Potts model as proposed by Alexander.²⁷

Above $1/3$ coverage the phase diagram is more complex and includes an incommensurate solid phase, a domain wall

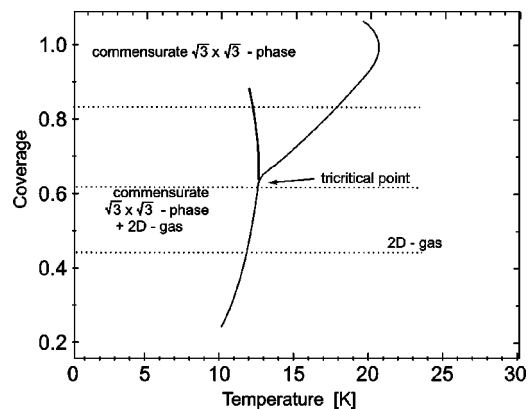


FIG. 1. The phase diagram of molecular hydrogen on graphite for coverages at and below the $1/3$ coverage where it forms the perfect $\sqrt{3} \times \sqrt{3}$ commensurate structure (Ref. 5). The coverage is expressed in units of $\rho_c = 0.0636 \text{ \AA}^{-2}$, the density of the complete $\sqrt{3} \times \sqrt{3}$ commensurate solid. The horizontal dashed lines denote cuts where the specific heat is computed by our PIMC method which is discussed in the following sections.

solid and a domain wall fluid phase.⁵ These phases have not been unequivocally characterized experimentally.

There are already certain theoretical studies of molecular hydrogen on graphite. Ni and Bruch,²⁸ using the Hartree-Jastrow approximation and the Lennard-Jones potential, calculated the ground state energy and the nearest-neighbor spacing for monolayer solids of H₂ adsorbed on the basal plane surface of graphite. Gottlieb and Bruch,^{29,30} using a Jastrow-variational approximation, calculated the energy and the structure of the commensurate and the domain-wall monolayer solids of molecular hydrogen adsorbed on graphite. Novaco³¹ calculated the ground state energy and density of states for the $\sqrt{3}\times\sqrt{3}$ commensurate solid phase of monolayer H₂ adsorbed on graphite using a self-consistent phonon approximation and investigated the effects of anisotropic admolecule-carbon interaction.

In this paper we present our results on submonolayer molecular hydrogen adsorbed on the basal plane surface of graphite using the path-integral Monte Carlo (PIMC) simulation method. Using the PIMC method³² and a given interaction model one can calculate, within only small statistical errors, the properties of a given number of boson particles (of the order of hundred or more), include the effects of permutations arising from the particle identity. A detailed outline of the application of PIMC to ⁴He systems can be found in Ref. 32. More recently this method has been extended to study quantum films similar to molecular hydrogen on graphite taking into account strong substrate corrugations.^{33,34} The PIMC simulation method has already been used to study molecular hydrogen systems. Examples of such applications are small clusters of parahydrogen molecules,^{35,36} bulk solid molecular hydrogen,^{37,38} the pure 2D system of hydrogen molecules,³⁹ and the surface melting of molecular hydrogen.⁴⁰

In this paper we have simulated molecular hydrogen on graphite using the semiempirical Silvera-Goldman potential^{41,42} for the interaction between two adsorbed molecules. For detemining the full interaction of a hydrogen molecule with the graphite we have used the Crowell-Brown model⁴³ for the H₂-carbon interaction and the expansion developed by Steele⁴⁴ and Carlos and Cole.⁴⁵ First we have considered a flat graphite substrate by taking the laterally averaged potential (ignoring substrate corrugations). We give a detailed analysis of the full phase diagram of a monolayer of molecular hydrogen on such a featureless graphite substrate up to first layer completion. However, the substrate corrugation plays a fundamental role in the formation of the $\sqrt{3}\times\sqrt{3}$ commensurate solid phase and the other phases which are defined by the presence of the substrate periodicity. Therefore, we have used the full interaction and we have studied the first layer up to 1/3 coverage. The results of our PIMC calculations for a corrugated substrate are given in Secs. IV–VII.

II. THE COMPUTATIONAL APPROACH

A. The interaction potential

In the simulation we assume that the H₂ molecules can be represented as spherical particles interacting with a semi-

empirical potential. We choose the form given by Silvera and Goldman⁴¹ for the interaction between two hydrogen molecules. The Silvera-Goldman model is a reliable potential for simulations at low temperatures and pressures.

The usual approach^{44,45} for evaluating the interaction $V(\mathbf{r})$ of a hydrogen molecule located at \mathbf{r} with the graphite surface assumes that it can be written as a sum of H₂-C interactions

$$V(\mathbf{r}) = \sum_i U(\mathbf{r} - \mathbf{X}_i). \quad (1)$$

The pair potential U is assumed centered at the equilibrium positions \mathbf{X}_i of the C atoms. Crowell and Brown⁴³ used the following anisotropic 6-12 potential to describe the interaction between a hydrogen molecule and a carbon atom on the graphite surface

$$U(\mathbf{r}) = -A \left[\frac{3}{4} (1 - \eta) \frac{\cos^2 \theta}{r^6} + \frac{1}{4} (1 + 5\eta) \frac{1}{r^6} - \left(1 + \frac{\eta}{2} \right) \frac{\sigma_{CH}^6}{r^{12}} \right], \quad (2)$$

where θ is the angle between the graphite c axis and the line joining the molecule and the carbon atom. The definitions and the values of parameters can be found in Ref. 43 $A = 3.469 \text{ \AA}^6$, $\eta = P_{\perp}/P_{\parallel} = 3.5$ is the ratio of the atomic polarizabilities perpendicular and parallel to the graphite c axis and for H₂ graphite. The $\sigma_{CH} = 3.25 \text{ \AA}$ is a length of the order of the core of the H₂-graphite interaction.

Following Steele⁴⁴ and Carlos and Cole⁴⁵ one can write the hydrogen graphite surface interaction as

$$V(\mathbf{r}) = V_0(z) + \sum_{\mathbf{G} \neq 0} V_{\mathbf{G}}(z) \exp(i\mathbf{G} \cdot \mathbf{R}), \quad (3)$$

where \mathbf{G} is a two-dimensional reciprocal lattice vector that corresponds to the graphite substrate surface and $\mathbf{R} = (x, y)$ is the projection of $\mathbf{r} = (x, y, z)$ on the surface plane.

Crowell and Brown⁴³ derived the laterally averaged interaction potential for a hydrogen molecule on the basal plane surface of graphite and the potential includes explicitly the anisotropy of carbon atoms in the graphite surface. Using the interaction (2) and the method developed by Steele^{44,45} they find

$$V_0(z) = - \frac{\pi \rho_s A}{h_0^4} \left(\frac{3}{8} (1 + \eta) \zeta(4, x) - \frac{\sigma_{CH}^6}{5x^{10} h_0^6} \left(1 + \frac{\eta}{2} \right) \right), \quad (4)$$

where $h_0 = 3.35 \text{ \AA}$, the distance between graphite basal planes, $\rho_s = 0.382 \text{ \AA}^{-2}$, the areal density of carbon atoms on the graphite surface. The variable $x = z/h_0$ and $\zeta(n, x) = \sum_{j=0}^{\infty} (j+x)^{-n}$ is a Riemann zeta function.

Using this laterally averaged potential for a hydrogen molecule on the graphite surface, a WKB method, and the renormalized Numerov technique, Crowell and Brown⁴³ have determined the bound state energy levels and compared

the results with experimental results. The discrepancy between calculated values and experimental values of the energy levels for the lower lying levels is about 6%.

Using the same interaction (2) and following closely the method developed by Steele⁴⁴ and extended by Carlos and Cole⁴⁵ one finds the following form for the corrugation amplitude:

$$V_G(z) = -A\pi\rho_s\beta_G \left(\frac{G^3}{128}(1-\eta) \frac{K_3(Gz)}{z} + \frac{1}{8}(1+5\eta) \right. \\ \left. \times \left(\frac{G}{2z} \right)^2 K_2(Gz) - \frac{\sigma_{CH}^6}{120} \left(1 + \frac{\eta}{2} \right) \left(\frac{G}{2z} \right)^5 K_5(Gz) \right), \quad (5)$$

where K_n are modified Bessel functions and

$$\beta_G = \exp(-i\mathbf{G} \cdot \mathbf{a}_1) + \exp(-i\mathbf{G} \cdot \mathbf{a}_2), \quad (6)$$

where \mathbf{a}_1 and \mathbf{a}_2 are the positions of two carbon atoms in the unit cell on the graphite surface.

B. PIMC method

Taking the previously mentioned interactions between hydrogen molecules and hydrogen-graphite into account we have used the same PIMC method developed by Pierce and Manousakis.^{33,34}

We have carried out two calculations: One is performed by using for the interaction of a hydrogen molecule and the graphite, the laterally averaged potential. The results obtained with this potential are given in the next section. In addition we have included the effects of the substrate corrugation by including the term given by Eq. (5). The results obtained with the full H_2 -graphite interaction are presented in Secs. IV–VII.

In the absence of the substrate corrugation amplitude, since the total potential is a spherically symmetric pair interaction, we use the matrix-squaring method in order to calculate the high temperature density matrix. The value of the imaginary time step used in this calculation is $\tau = 1/(120 \text{ K})$. We have used $l=2$ level bisection while the $l=3$ level gave too low acceptance ratio in this case.

In order to simulate the first layer with the substrate corrugation, we have used the so-called semiclassical approximation for the expression for small τ (high temperature) of the part of the density matrix³³ associated with the anisotropic interaction of a hydrogen molecule with the graphite surface. Part of our PIMC simulation method is the multi-level Metropolis method.³³ In the multilevel bisection method it is important to choose the best value of l . We have used $l=2$ for the calculations with the laterally average potential and $l=3$ for the calculation with corrugations. We have computed expectation values for the total energy, the static structure factor, the probability distribution, the density profile and the specific heat. To thermalize the system, we typically carried out of the order of 15 000 MC steps. After the thermalization process we carried out of the order of 20 000 MC steps in order to compute observables.

Before we began our investigation of the adsorption of molecular hydrogen films on graphite, we checked our program using various tests, one of which was the following. Crowell and Brown⁴³ calculated the bound state energy levels using the same laterally averaged potential. They solved the Schrödinger equation using a WKB method and the renormalized Numerov technique and they quoted a single molecule-substrate binding energy of approximately -455 K . In PIMC we can easily compute the single particle binding energy E_B to the graphite surface by simulating one hydrogen molecule on graphite. Our calculated value at $T = 0.8 \text{ K}$ is $E_B = -452.6 \pm 0.1 \text{ K}$. If this result of our calculation is extrapolated to zero temperature it should be lowered by an amount of the order of 1 K. Any additional small difference is due to the finite-size substrate used in our calculation (we used a $21.03 \text{ \AA} \times 24.283 \text{ \AA}$ size substrate) which raises the H_2 kinetic energy of the H_2 molecule.

III. FIRST LAYER WITHOUT SUBSTRATE CORRUGATION

In this section, we neglected the substrate corrugation amplitude $V_G(z)$ and used only the laterally averaged portion $V_0(z)$ of the interaction of a hydrogen molecule with the graphite surface. As shown in the next section, the substrate corrugation amplitude plays an important role on the phase diagram of the monolayer. Due to the strong influence of the substrate corrugation potential, the monolayer exhibits a $\sqrt{3} \times \sqrt{3}$ commensurate solid phase at low coverages and undergoes a commensurate-incommensurate transition via a formation of domain-wall phases at higher coverages.

We expect that the phase diagram of the monolayer without the substrate corrugation to be similar to that of the pure 2D hydrogen film.³⁹ Helium on a smooth graphite surface using a laterally averaged potential has been simulated by Whitlock, Chester, and Krishnamachari⁴⁶ using Green-function Monte Carlo and by Pierce and Manousakis⁴⁷ using the PIMC method. The phase diagram of helium on the smooth graphite surface is similar to the pure 2D helium film.⁴⁸

Gordillo and Ceperley³⁹ studied a pure 2D system of hydrogen molecules and calculated the total energy per hydrogen molecule and the static structure factor $S(k)$ as a function of molecular hydrogen coverage. They found a minimum energy at the coverage $\rho = 0.064 \text{ \AA}^{-2}$ where the 2D molecular hydrogen film has a solid phase. The static structure factor has one sharp peak at $k = 1.7 \text{ \AA}^{-1}$ corresponding to a triangular lattice. They also found a fluid phase for $\rho < 0.059 \text{ \AA}^{-2}$.

In our simulations we input the total number of particles, the area of the simulation cell, and the temperature in each run. We kept the size of the simulation cell constant and changed the total number of particles in order to vary the density. The size of the simulation cell has been chosen so that the cell can accommodate the periodic structure of a triangular solid phase because we expect that the monolayer of molecular hydrogen has a triangular solid phase just before the first layer is complete. We have used a rectangular

TABLE I. Energy per hydrogen molecule versus density for the first layer without the substrate corrugation. The simulation cell is $21.03 \text{ \AA} \times 24.283 \text{ \AA}$. The number in parentheses gives the error in the last decimal place(s).

$\rho(\text{\AA}^{-2})$	$E/N(K)$	$\rho(\text{\AA}^{-2})$	$E/N(K)$
0.0020	-452.588(61)	0.0705	-477.500(72)
0.0196	-465.045(96)	0.0744	-475.424(41)
0.0294	-468.698(40)	0.0783	-473.096(27)
0.0392	-470.111(62)	0.0822	-466.984(17)
0.0490	-472.527(37)	0.0861	-461.206(25)
0.0587	-475.917(23)	0.0881	-456.539(131)
0.0627	-475.893(50)	0.0901	-453.588(17)
0.0646	-476.074(37)	0.0920	-451.467(41)
0.0666	-476.259(30)	0.0940	-450.791(26)
0.0685	-476.562(5)	0.0960	-444.780(58)

simulation cell with dimensions $21.03 \text{ \AA} \times 24.28 \text{ \AA}$ and applied periodic boundary conditions in the x - y plane.

We have calculated the total energy per hydrogen molecule as a function of hydrogen coverage at 1 K. The values for the total energy per hydrogen molecule are given in Table I. The minimum energy is $e_0 = -477.50(7) \text{ K}$ at the equilibrium density $\rho_0 = 0.0705 \text{ \AA}^{-2}$. For a pure 2D system of hydrogen molecules, the density with the lowest energy per hydrogen molecule is 0.064 \AA^{-2} ,³⁹ lower than our result. This can be easily understood by the fact that confining the system in strictly 2D increases the kinetic energy due to the additional zero point motion.

In Fig. 2 we give the total energy as a function of hydrogen coverage at 1 K. We shifted the total energy by subtracting a value of Ne_0 , where N is the number of hydrogen molecules and e_0 is the minimum energy per hydrogen molecule. As the solid-gas coexistence phase is unstable, the total energy in the coexistence region between two stable

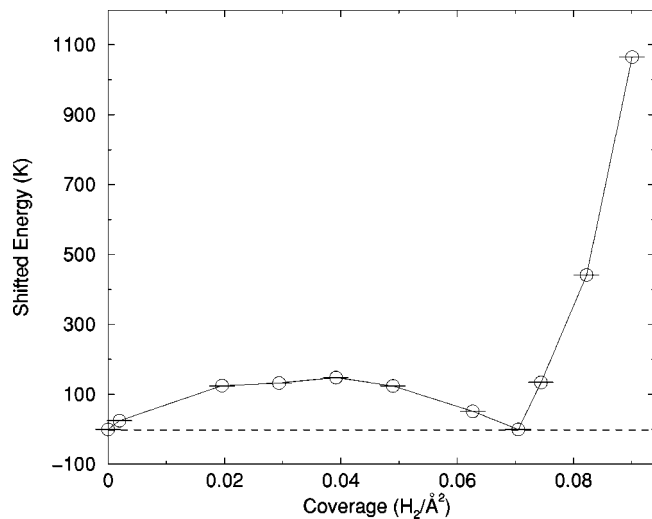


FIG. 2. Total energy as a function of coverage on the smooth graphite substrate at $T=1 \text{ K}$. The energy is shifted by Ne_0 , where N is the number of hydrogen molecules and $e_0 = -477.50(7) \text{ K}$, the minimum energy per hydrogen molecule.

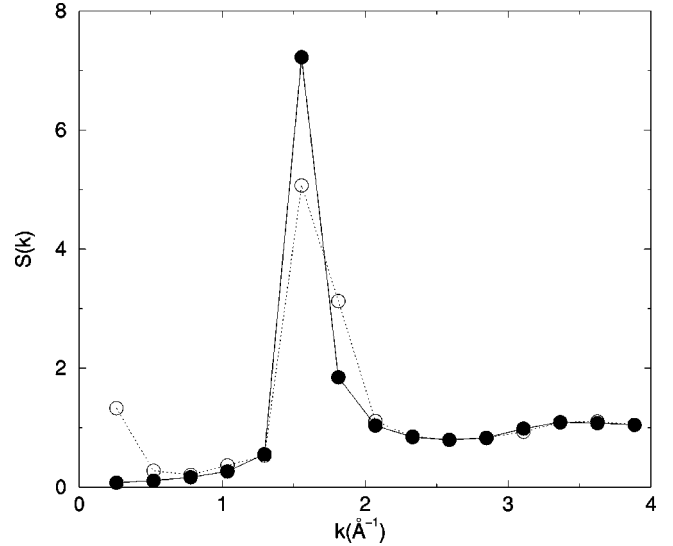


FIG. 3. Static structure factor $S(k)$ at the coverages 0.0490 (filled circles) and 0.0588 (open circles) \AA^{-2} and at $T=1 \text{ K}$. These coverages are in the coexistence region. At the lowest density $S(k)$ bends upward for low values of k .

phases (a gas phase and a solid phase) has an upward curvature. It is evident from Fig. 2 that the energy values are above the straight line from zero density to the minimum energy density ρ_0 . Thus, for densities between zero coverage and the equilibrium density ρ_0 there is a solid-gas coexistence region. In the density region above ρ_0 the system is in a solid phase as demonstrated next.

We have calculated the structure factor $S(k)$ shown in Fig. 3. At the lowest density, $S(k)$ has a peak at $k = 1.55 \text{ \AA}^{-1}$ and bends upward for low values of k instead of going to zero. This indicates that we have a mixture of solid and gas and that we observe a solid-gas coexistence phase. The static structure factor at the equilibrium coverage is shown in Fig. 4. It has just a single sharp peak at $k = 1.79 \text{ \AA}^{-1}$. This indicates that the molecular hydrogen adsorbed on graphite forms an equilateral triangular solid phase. For 2D molecular hydrogen films the static structure factor at the equilibrium density has a solid structure factor with also a single sharp peak at a smaller value $k = 1.7 \text{ \AA}^{-1}$.³⁹ In Fig. 4 we also show the static structure factor at the promotion density, $0.094 \text{ atom/\AA}^{-2}$ where we also find a single sharp peak at $k = 2.07 \text{ \AA}^{-1}$. The solid phase at this density is an equilateral triangular solid phase and the nearest-neighbor distance of hydrogen molecules is 3.505 \AA .

We have calculated the pair distribution functions $g(r)$ at the solid-gas coexistence region, at the equilibrium density, and well inside the solid region. Here, $r = |\mathbf{R}|$ is the magnitude of the projection of the distance vector between two particles onto the plane of the substrate. For the three lower coverages, the first peaks are located at the same value of r as shown in Fig. 5. This indicates that the average separation distance of nearest neighbor particles in the coexistence region is close to the one at the equilibrium coverage. However, for densities above the equilibrium coverage the first

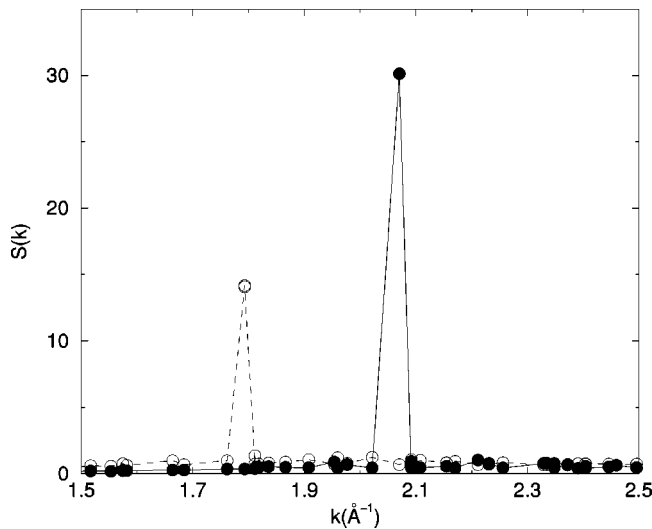


FIG. 4. Static structure factor $S(k)$ at the equilibrium density (open circles) and the completion density of the first layer (filled circles) and at $T=1$ K. The peak positions are $k=1.79$ and 2.07 \AA^{-1} , respectively.

peak's position is shifted from 3.759 to 3.379 \AA as shown in Fig. 6.

In Fig. 7 we give the contour plot of the probability distribution for the density $\rho=0.0294 \text{ \AA}^{-2}$. As we have discussed, for this coverage the system is in the solid-gas coexistence region. The figure shows a snapshot of the solid-gas coexistence phase. The hydrogen molecules form a cluster which incompletely covers the substrate surface area. The contour plot of the probability distribution at the equilibrium density is shown in Fig. 8 where an equilateral triangular solid phase is clearly seen. Figure 9 shows the contour plot of the probability distribution at the density 0.0940 \AA^{-2} . The hydrogen molecules also form a triangular lattice and

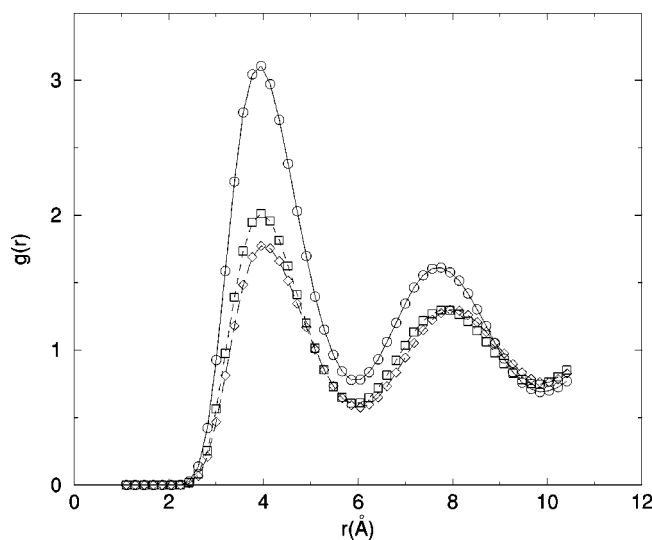


FIG. 5. The radial distribution function $g(r)$ at $T=1$ K and at densities 0.0294 (circles), 0.0490 (squares), and 0.0588 (diamonds), all of which are below the equilibrium density. The first peak is located at the same value of r for the three values of the density.

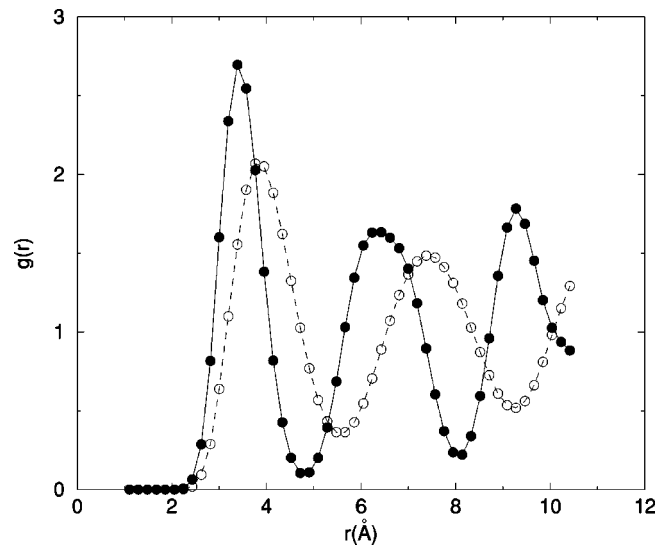


FIG. 6. The radial distribution function $g(r)$ at the equilibrium density (open circles) and the completion density of the first layer (filled circles) and at $T=1$ K. The first peak position moves from 3.759 to 3.379 \AA .

they are closer together at nearest neighbor distance of $r_{NN}=3.505 \text{ \AA}$.

From the density profile $\rho(z)$ we can determine the density where the first layer is complete and the second layer starts to form. The density profiles for three densities are shown in Fig. 10. The coverage $\rho=0.094 \text{ \AA}^{-2}$ shows no evidence of promotion. The beginning formation of the sec-

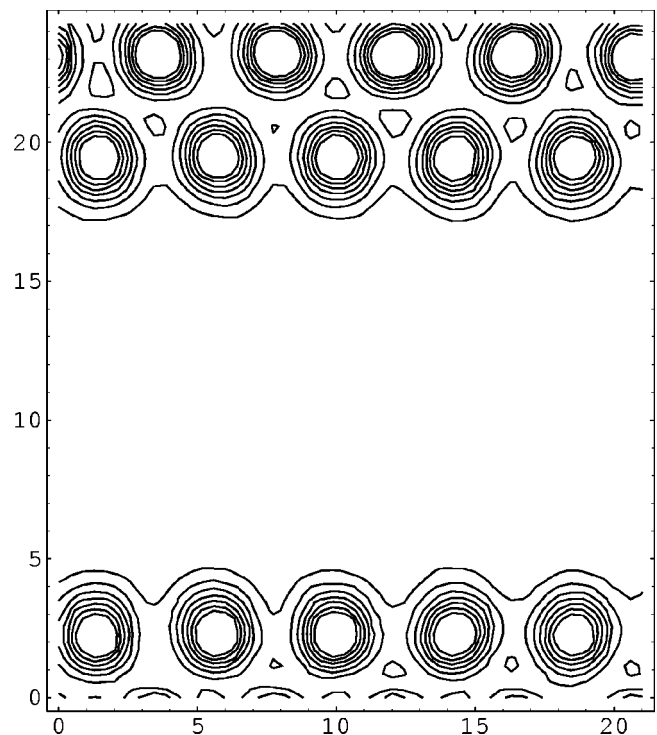


FIG. 7. Contour plot of the probability distribution at the density 0.0294 \AA^{-2} for $T=1.0$ K. The hydrogen molecules incompletely cover the substrate.

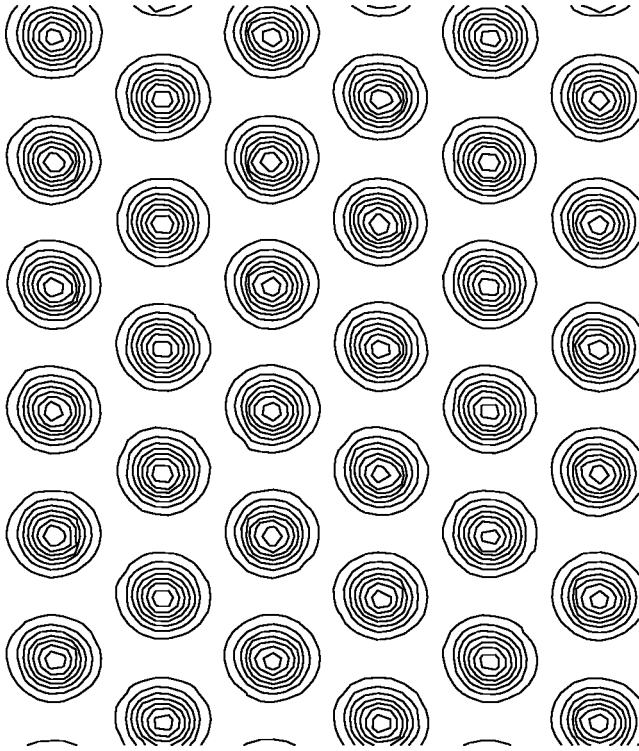


FIG. 8. Contour plot of the probability distribution at the equilibrium density 0.0705 \AA^{-2} for $T=1.0 \text{ K}$. It forms an equilateral triangular solid phase.

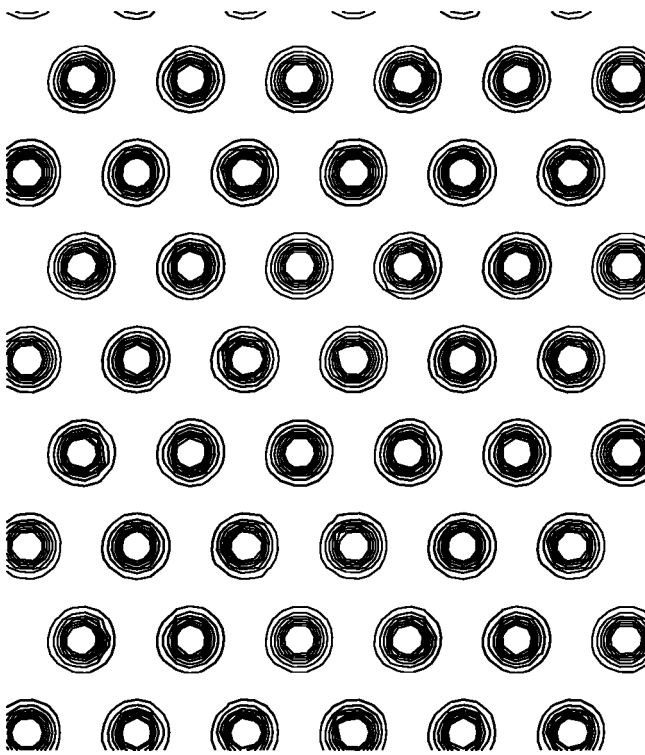


FIG. 9. Contour plot of the probability distribution at the completion density of the first layer 0.0940 \AA^{-2} for $T=1.0 \text{ K}$. It forms an equilateral triangular solid phase.

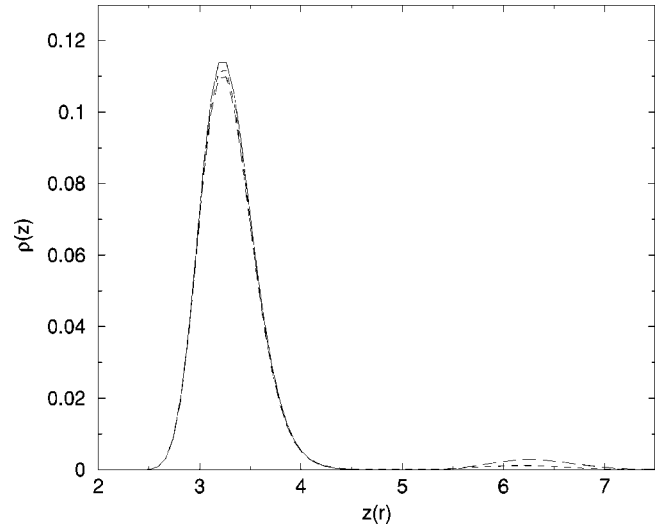


FIG. 10. Density profiles at $T=1 \text{ K}$ and for several coverages: 0.094 \AA^{-2} (solid line), 0.0960 \AA^{-2} (dashed line), and 0.0979 \AA^{-2} (long-dashed line). The coverage 0.094 \AA^{-2} shows no evidence of promotion. The beginning of formation of the second layer is clearly visible at the higher densities.

ond layer is clearly visible at the densities $\rho=0.0960$ and $\rho=0.0979 \text{ \AA}^{-2}$. Thus, the promotion density is approximately $\rho=0.094 \text{ \AA}^{-2}$, which is the same as the experimental value.

IV. FIRST LAYER WITH SUBSTRATE CORRUGATION

An ideal basal plane of graphite consists of open hexagons with each carbon atom having three nearest neighboring carbon atoms. The graphite substrate corrugation potential is relatively strong for physisorption but is short ranged perpendicular to the substrate. Near the graphite surface the effect of the substrate corrugation on the phase diagram of the first layer has to be taken into account. It is well known that commensurate monolayer solids of helium adsorbed on graphite are directly related to the substrate corrugation amplitude $V_G(z)$ of the helium-substrate holding potential.^{33,47,49,50} In the following three sections, we will present our results for the first layer when we use a molecule-graphite potential which includes the laterally averaged potential given by Eq. (4) and part given by Eq. (5) which gives the substrate corrugation.

We have used $\tau=1/(200 \text{ K})$ in the calculations of this part. We have implemented a variety of simulation cells that are appropriate for examining different phase regions of the phase diagram. We have applied periodic boundary conditions in the x and y directions.

The $\sqrt{3} \times \sqrt{3}$ COMMENSURATE SOLID PHASE

In order to accommodate the periodicity of the adsorption sites of graphite and the $\sqrt{3} \times \sqrt{3}$ commensurate solid phase, we have chosen the simulation cell with dimensions $x=6\sqrt{3} a_{gr}$ and $y=15 a_{gr}$, where $a_{gr}=2.459 \text{ \AA}$ is the distance between the centers of two neighboring hexagons on

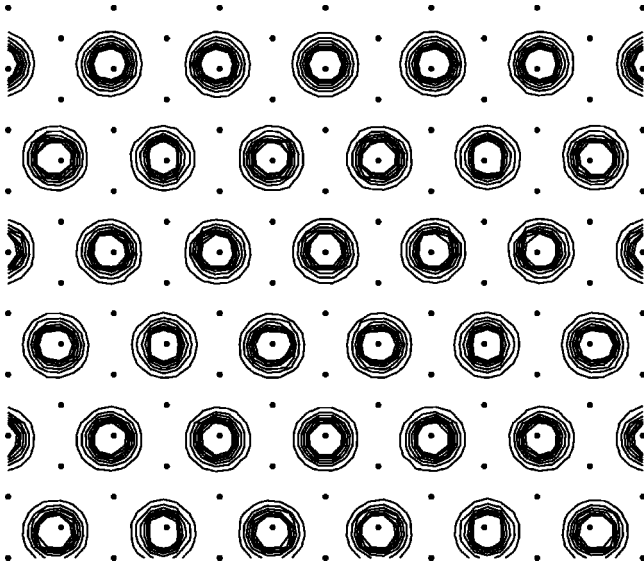


FIG. 11. Contour plot of the probability distribution at the commensurate solid phase density 0.0636 \AA^{-2} for $T=1.33 \text{ K}$. The filled circles indicate graphite adsorption sites. Hydrogen molecules occupy one-third of all the potential minima. Molecules form a triangular solid lattice with 4.26 \AA nearest neighboring spacing.

the graphite surface. This cell can accommodate 60 hydrogen molecules at the $\sqrt{3} \times \sqrt{3}$ commensurate solid density. We kept the size of the simulation cell constant and changed the number of particles in order to vary the density. At exactly $1/3$ coverage, which corresponds to an areal density of $\rho = 0.0636 \text{ \AA}^{-2}$, we find a $\sqrt{3} \times \sqrt{3}$ commensurate solid structure. In Fig. 11 we give the contour plot of the probability distribution of H_2 molecules on graphite. The dots denote graphite- H_2 potential energy minima. Notice that the H_2 molecules occupy one-third of all the possible adsorption sites and they form a $\sqrt{3} \times \sqrt{3}$ solid.

At high temperature (above 20 K) this commensurate solid melts to a fluid of molecules uniformly distributed on the surface of graphite. Structure factors and other observables have been calculated and are shown in the following section.

VI. COMMENSURATE SOLID CLUSTERS

Below the $1/3$ coverage and at low temperature we find that the system exists in a phase consisting of $\sqrt{3} \times \sqrt{3}$ commensurate solid clusters surrounded by vapor. In this coexistence phase as the density increases hydrogen molecules condense from the vapor phase to this commensurate solid structure.

We have calculated the total energy of the first layer at practically zero temperature in order to determine the coverage range of the commensurate solid-vapor coexistence phase using the Maxwell construction, which can be used to identify the unstable regions.

The values for the total energy per hydrogen molecule are given in Table II for several coverages. The minimum energy per hydrogen molecule is $e_{\min} = -476.88 \pm 0.05 \text{ K}$ and occurs at the $\sqrt{3} \times \sqrt{3}$ commensurate solid density ρ_c

TABLE II. Energy per hydrogen molecule versus density for interaction with the substrate corrugation. The simulation cell is $25.554 \text{ \AA} \times 36.885 \text{ \AA}$. The number in parentheses gives the error in the last decimal place(s).

$T(\text{K})$	$\rho(\text{\AA}^{-2})$	$E/N(\text{K})$
1.333	0.0318	-470.307(31)
1.333	0.0424	-471.983(22)
2.000	0.0530	-473.328(27)
2.000	0.0636	-476.879(45)
2.000	0.0678	-471.518(25)
2.000	0.0721	-468.903(69)
2.000	0.0763	-464.781(67)
2.000	0.0806	-459.141(14)
2.000	0.0848	-450.492(71)
2.000	0.0890	-440.143(19)

$= 0.0636 \text{ \AA}^{-2}$. In Fig. 12 we give the shifted total energy as a function of hydrogen molecule density. The energy values are shifted by $e_{\min}N$, where N is the number of hydrogen molecules in the simulation. If we draw a line from zero density to the commensurate solid density ρ_c , all intermediate energy values are above the line. This means that the energy values between zero density and the $\sqrt{3} \times \sqrt{3}$ commensurate solid density are unstable and a phase separation occurs at these densities. A commensurate solid-vapor coexistence phase occurs between zero density and the $\sqrt{3} \times \sqrt{3}$ commensurate solid density $\rho_c = 0.0636 \text{ \AA}^{-2}$ and is followed by the $\sqrt{3} \times \sqrt{3}$ commensurate solid phase at ρ_c .

In order to find out if the first layer has a commensurate solid-gas coexistence phase and a $\sqrt{3} \times \sqrt{3}$ commensurate solid phase for our determined coverages, we have computed the probability distribution and the static structure factor $S(k)$. For these calculations we have chosen the simulation cell with dimension $x = 6\sqrt{3} a_{\text{gr}}$ and $y = 9a_{\text{gr}}$.

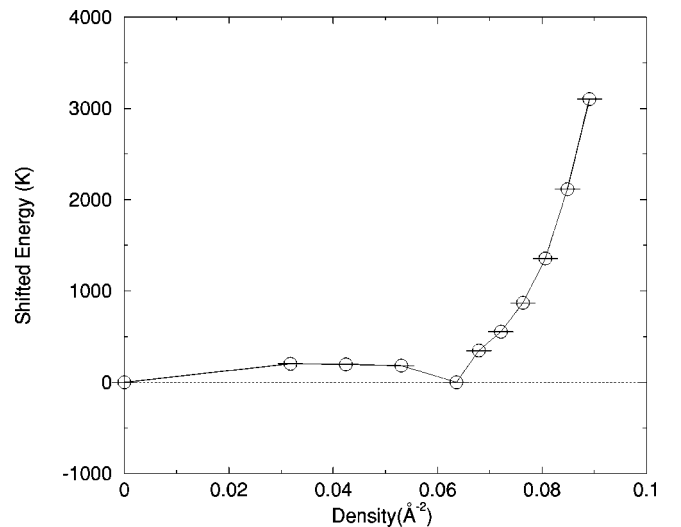


FIG. 12. Total energy versus density with the substrate corrugation. The energy is shifted by a value of Ne_0 , where N is the number of hydrogen molecules and $e_0 = -476.879(45)$, the minimum energy per hydrogen molecule.

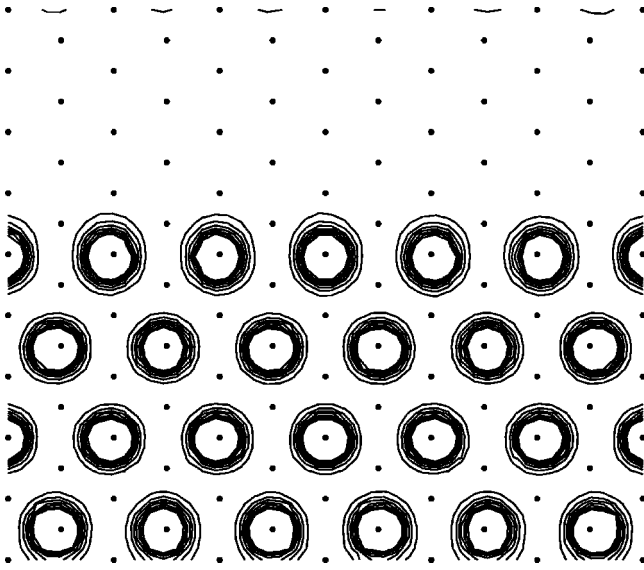


FIG. 13. Contour plot of the probability distribution at the density 0.0424 \AA^{-2} for $T=1.0 \text{ K}$. The filled circles indicate graphite adsorption sites. Hydrogen molecules are located near the potential minima. The commensurate solid phase is separated from the vapor phase by a boundary layer.

In Fig. 13, the contour plot of the probability density is presented for a temperature 1.0 K and for coverage 0.0424 \AA^{-2} . In this figure, filled circles indicate adsorption sites of graphite. We see a commensurate solid phase coexisting with the gas phase. In Fig. 13 a commensurate solid phase is formed in the bottom and a gas phase is formed on the top. In this case because the temperature is low the vapor phase has no molecules. Notice that as in the $\sqrt{3} \times \sqrt{3}$ commensurate solid phase shown in Fig. 11, hydrogen molecules, in the lower part of the periodic substrate of Fig. 13, also occupy one-third of all the adsorption sites of graphite. This demonstrates directly that below $1/3$ coverage and at low temperature the system forms a $\sqrt{3} \times \sqrt{3}$ commensurate-solid phase surrounded by vapor.

In order to obtain some information on the structure for each phase, we have calculated the static structure factor $S(k)$ at the density $\rho_c = 0.0636 \text{ \AA}^{-2}$ of the $\sqrt{3} \times \sqrt{3}$ commensurate solid phase and densities below ρ_c . The static structure factors $S(k)$ are shown in Fig. 14. The first peak for the three cases shown are at the same position and the peak heights of the static structure factor increase as the density increases. The peak's positions are $k = 1.70 \text{ \AA}^{-1}$ and $k = 3.40 \text{ \AA}^{-1}$. This means that the phases have the $\sqrt{3} \times \sqrt{3}$ commensurate solid structure and it is exactly what has been observed experimentally by neutron scattering. In the $\sqrt{3} \times \sqrt{3}$ commensurate solid phase, the nearest-neighbor spacing of hydrogen molecules is 4.26 \AA corresponding to $k = 1.70 \text{ \AA}^{-1}$.

For coverages below the $\sqrt{3} \times \sqrt{3}$ commensurate solid density ρ_c , the static structure factors $S(k)$ do not go to zero as k approaches zero. This is due to the fact that the solid phase has a finite spatial extent due to the phase coexistence with the gas phase.

In order to study the melting of the commensurate solid

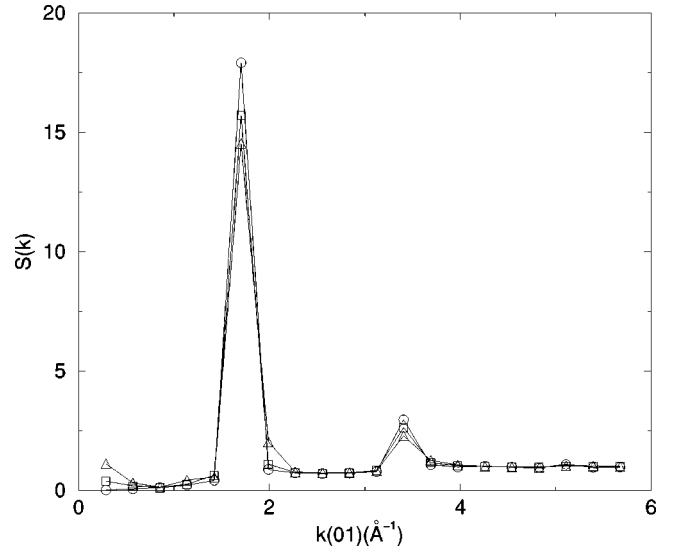


FIG. 14. Static structure factor $S(k)$ at the densities 0.0530 (triangles), 0.0566 (squares), 0.0636 \AA^{-2} (circles). The number of particles are 30, 32, and 36, respectively.

cluster phase, we have computed the specific heat for several temperatures. The specific heat can be calculated by differentiating the total energy value with respect to the temperature. At the melting temperature the specific heat has a maximum and a peak in plotting the values of the specific heat as a function of temperature. We have calculated the specific heat at the densities 0.0281 \AA^{-2} and 0.0390 \AA^{-2} (these temperature scans are shown in Fig. 1 by the two lower horizontal dotted lines). We make use of the simulation cells with dimensions $42.59 \text{ \AA} \times 44.262 \text{ \AA}$ and $38.332 \text{ \AA} \times 36.885 \text{ \AA}$, respectively. The values of the total energy per hydrogen molecule are given in the Table III. Figures 15 and 16 show the temperature dependence of the specific heat.

TABLE III. Total energy per hydrogen molecule at the densities 0.0281 and 0.039 \AA^{-2} . The number in parentheses gives the error in the last decimal place(s).

$T(K)$	$\rho = 0.0281 \text{ \AA}^{-2}$	$\rho = 0.039 \text{ \AA}^{-2}$	
	$E/N(K)$	$T(K)$	$E/N(K)$
5.714	-469.810(80)	6.667	-470.388(50)
6.667	-468.845(169)	6.897	-470.081(132)
7.143	-467.428(228)	7.143	-469.862(113)
7.692	-466.409(231)	7.407	-469.241(116)
8.0	-465.359(214)	7.692	-469.109(89)
8.333	-463.979(188)	8.000	-468.529(143)
9.091	-460.847(144)	8.333	-467.590(204)
10.0	-458.263(112)	8.696	-465.993(256)
11.111	-456.138(140)	9.091	-464.814(271)
12.50	-454.301(82)	9.524	-463.079(173)
		10.00	-461.799(138)
		11.111	-459.890(96)
		12.500	-457.945(74)
		14.286	-455.884(23)

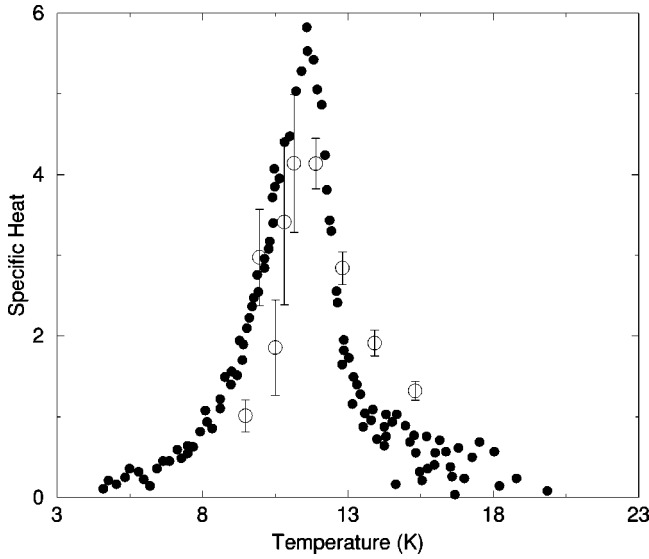


FIG. 15. Specific heat versus temperature at the density 0.0281 \AA^{-2} . The filled circles are the experimental data at the same density. The results of our calculation have been shifted by 2.8 K along the temperature axis.

The values used in the figures are given in Table IV. The filled circles in the figures correspond to the experimental specific-heat values¹⁻³ at the same density. Our estimated melting temperatures are lower than the experimental results. In order to compare our computed specific heat with the experimental specific heat, our results have been shifted by the amounts of 2.8 and 3.4 K in the temperature axis. This disagreement may be attributed to both finite-size effects and to the hydrogen-graphite interaction. Notice, however that basic characteristics of the specific heat such as the location of the peak, the peak height and its width and their temperature dependence are well reproduced with no free parameters.

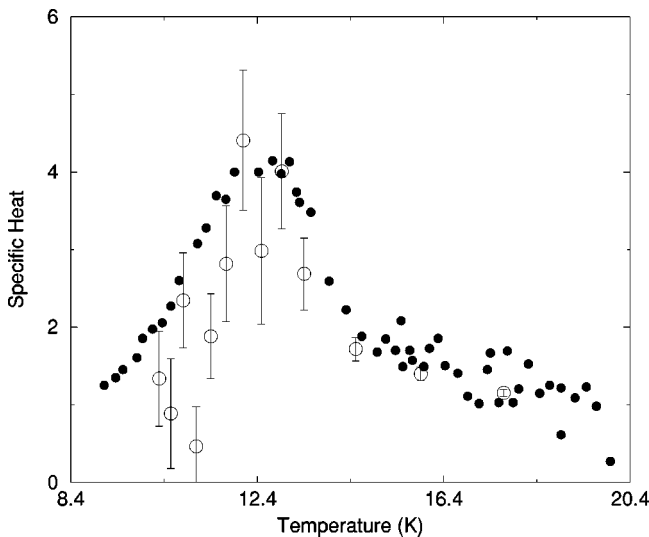


FIG. 16. Specific heat versus temperature at the density 0.039 \AA^{-2} . The filled circles are the experimental data at the same density. The results of our calculation have been shifted by 3.4 K along the temperature axis.

TABLE IV. Specific heat at the densities 0.0281 and $0.0390 \text{ H}_2/\text{\AA}^2$. The number in parenthesis gives the error in the last decimal place(s).

$\rho = 0.0281 \text{ H}_2/\text{\AA}^2$		$\rho = 0.039 \text{ H}_2/\text{\AA}^2$	
$T(K)$	C/Nk_B	$T(K)$	C/Nk_B
6.667	1.014(197)	6.897	1.337(613)
7.143	2.975(596)	7.143	0.888(706)
7.692	1.855(591)	7.407	2.346(613)
8.0	3.413(1024)	7.692	0.466(513)
8.333	4.140(856)	8.000	1.884(546)
9.091	4.134(313)	8.333	2.818(746)
10.0	2.843(201)	8.696	4.407(903)
11.111	1.913(161)	9.091	2.984(943)
12.50	1.323(117)	9.524	4.008(742)
		10.00	2.687(465)
		11.111	1.719(152)
		12.500	1.400(88)
		14.286	1.154(44)

These calculations were performed on a special purpose 32-node 64 processor machine (built by one of the authors, see HRL <http://stratos.fsu.edu>) dedicated for more than a year to this calculation. Unfortunately taking the thermodynamic limit (i.e., studying the dependence of our results to the system size and from that to take the infinite size limit) requires computational resources far beyond what is realistically available. However, we expect and we found that by increasing the system size the critical temperature increases and this reduces the disagreement with the experiment.

As the temperature increases, the system undergoes a transition from a commensurate solid cluster phase to a 2D gas phase at the melting temperature (the location of the specific heat peak). In Fig. 17 we present the contour plot of the probability distribution at the temperatures $T = 6.67 \text{ K}$ and $T = 12.5 \text{ K}$ at the density $\rho = 0.0396 \text{ \AA}^{-2}$. At the higher temperature all the adsorption sites of graphite are occupied with equal probability.

VII. COMMENSURATE SOLID WITH VACANCIES

A single peak occurs in the specific heat as a function of temperature at low densities as shown in the previous sec-

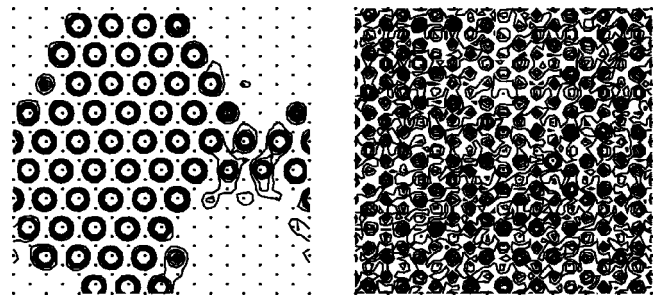


FIG. 17. Contour plot of the probability distribution at the density 0.0396 \AA^{-2} for $T = 6.67 \text{ K}$ and $T = 12.5 \text{ K}$. At higher temperature all the adsorption sites of graphite are occupied with equal probability.

TABLE V. Total energy per hydrogen molecule and specific heat at the density 0.0519 \AA^{-2} . The number in parenthesis gives the error in the last decimal place(s).

$T(K)$	$E/N(K)$	C/Nk_B
6.667	-472.508(80)	
7.143	-472.244(30)	0.553(180)
7.692	-471.633(136)	1.113(253)
8.333	-470.812(58)	1.281(230)
8.696	-470.372(81)	1.214(274)
9.091	-469.387(148)	2.492(426)
9.524	-468.502(144)	2.044(478)
10.0	-467.073(172)	3.000(471)
11.111	-464.194(111)	2.591(184)
11.765	-462.897(75)	1.985(204)
12.50	-461.810(13)	1.478(103)
13.333	-460.784(28)	1.231(37)
14.286	-459.712(32)	1.126(44)
16.667	-457.166(39)	1.069(21)
20.0	-453.660(51)	1.052(19)

tion. At higher coverages below the $\sqrt{3} \times \sqrt{3}$ commensurate solid density and above the tricritical point (which corresponds to an approximate coverage of $\sim 0.65\rho_c$), the specific heat has two anomalies. We computed the specific heat at the density 0.0519 \AA^{-2} for several values of the temperature (this temperature scan is shown in Fig. 1 by the upper dotted line). The total energy per hydrogen molecule and the specific heat are given in Table V. The specific heat as a function of temperature is compared to the experimental results¹⁻³ (filled circles) in Fig. 18. The transition from the commensurate solid-vapor coexistence phase to the uniform commensurate solid phase occurs at around 8 K and the transition from the commensurate solid phase to the gas phase occurs at around 10 K. Our critical temperatures are lower

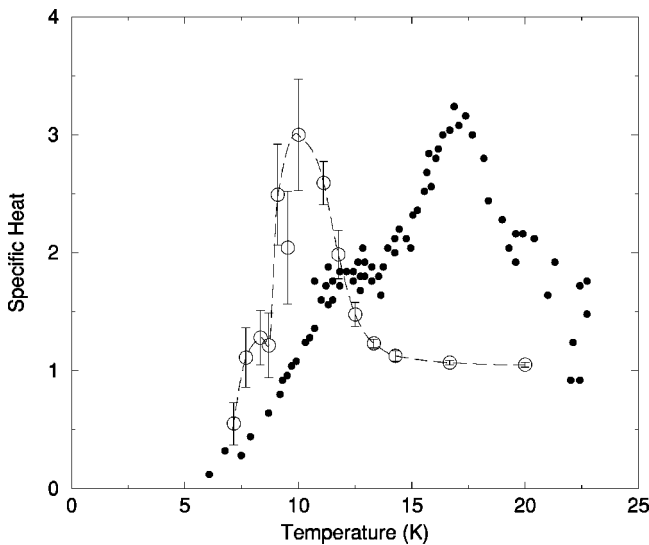


FIG. 18. Specific heat versus temperature at the density 0.0519 \AA^{-2} . The filled circles are the experimental data at the same density.

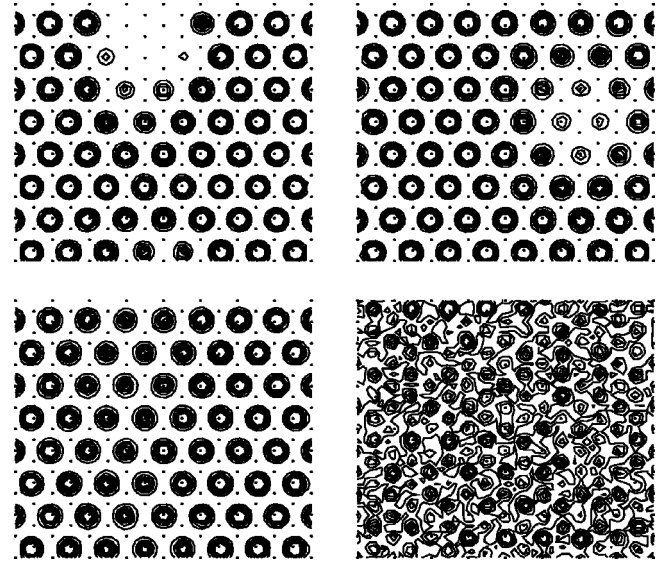


FIG. 19. Contour plot of the probability distribution at the density 0.0519 \AA^{-2} at various values of temperature. The plots shown are (a) top row left, $T=6.67 \text{ K}$; (b) top row right, $T=8.33 \text{ K}$; (c) bottom row left, $T=9.09$; (d) bottom row right, $T=13.33 \text{ K}$.

than the experimental data for two main reasons. First finite-size effects tend to reduce the transition temperature. Second our H_2 -graphite interaction potential is somewhat weaker than the true interaction. The potential we used gives a binding energy for a single molecule with the substrate of about 455 K which is smaller than the measured value of 483 K.⁵¹ We computed the probability distribution and the static structure factor $S(k)$ at the three different regions. In Fig. 19 we give the contour plot of the the probability distribution for different temperature values. Notice that we can identify three different phases in this figure: a commensurate solid cluster phase which forms at low temperature; the contour plot that corresponds to $T=9.09 \text{ K}$ shows the presence of

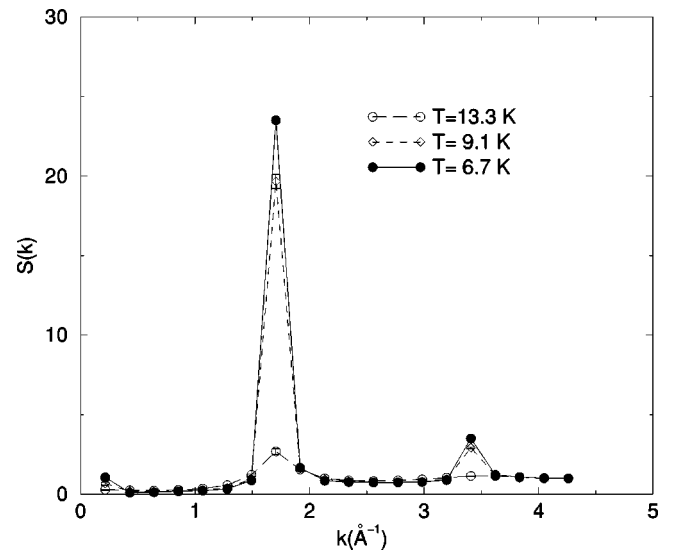


FIG. 20. Static structure factor $S(K)$ for three different values of temperature at the density 0.0519 \AA^{-2} .

the commensurate solid phase with vacancies; at temperature higher than 10 K for this density we can identify the gas phase. The static structure factor is given in Fig. 20. From this figure it appears that the vacancies are uniformly distributed inside the solid. Our simulation indicates that the vacancy mobility in the commensurate solid is low which makes the simulation of this phase difficult because of very long relaxation time scales.

VII. SUMMARY

Submonolayer molecular hydrogen on the graphite basal plane surface is a strongly correlated 2D system where quantum fluctuations are large because of the low molecular mass, weak Van der Waals interactions and reduced dimensionality. Nevertheless the system avoids states which are the product of quantum fluctuations and exhibits a phase diagram which has an analogy in classical 2D systems. However, to quantitatively understand these phases one needs to use full quantum statistical mechanics. We have used the PIMC method to study the submonolayer phase diagram at or below the $1/3$ coverage where it forms a $\sqrt{3}\times\sqrt{3}$ commensurate solid. We have been able to verify most of the features of the experimentally determined phase diagram.⁵ Our approach is limited by the interaction potentials used and by the finite-size effects. Due to the fact that we treat all the quantum mechanical effects including the effects of particle permutations exactly, we can only simulate systems involving of the order of 100–200 H_2 molecules. Our approach, however, gives direct information on the molecule-molecule correlations and structures formed on the surface.

We have computed the total energy as a function of coverage, the molecular pair distribution function, structure factors, molecular probability distribution, density profile as a function of the distance from the graphite surface, and the specific heat as a function of temperature for various coverages. We have carried out two different calculations: (a) one

using only a laterally averaged potential and (b) another where we have taken into account the effects of substrate corrugation. For the latter we used a form for the H_2 -graphite interaction similar to the Carlos-Cole⁴⁵ potential for the He-graphite interaction, but appropriate for the H_2 -graphite case.

In the case of the flat substrate, using the laterally averaged potential, we carried our calculations up to a coverage where the first layer is completed and the next layer starts to form. We found that the first layer has a solid-gas coexistence phase at low densities and a triangular solid phase at and above the equilibrium density $\rho_0=0.0705 \text{ \AA}^{-2}$. We also find a layer promotion density of 0.094 \AA^{-2} which is in good agreement with the experiment. In order to investigate the commensurate solid formation and structure we need to take into account the effects of substrate corrugations. When we do that we find that at low temperature below a critical density the system forms a mixture of a phase of $\sqrt{3}\times\sqrt{3}$ commensurate solid clusters and a vapor phase. Staying below this critical density and by raising the temperature the clusters undergo melting at a definite temperature giving rise to a specific heat peak. At densities greater than this critical density and below $1/3$ coverage we find that the specific heat has two anomalies as a function of temperature. At low temperature the system is in the same mixed phase as in the low density region. As the temperature becomes higher than a coverage-dependent critical temperature, the system transforms into a single phase, a $\sqrt{3}\times\sqrt{3}$ commensurate solid with vacancies. Above another characteristic coverage-dependent temperature, the commensurate solid melts into a uniform fluid.

ACKNOWLEDGMENTS

This work was supported by the National Aeronautics and Space Administration under Grant Nos. NAG3-1841 and NAG8-1773.

-
- ¹M. Bretz and T.T. Chung, *J. Low Temp. Phys.* **17**, 479 (1974).
²F.C. Motteler and J.G. Dash, *Phys. Rev. B* **31**, 346 (1985).
³F.A.B. Chaves, M.E.B.P. Cortez, R.E. Rapp, and E. Lerner, *Surf. Sci.* **150**, 80 (1985).
⁴H. Freimuth and H. Wiechert, *Surf. Sci.* **162**, 432 (1985).
⁵H. Wiechert, *Physica B* **169**, 144 (1991).
⁶H. Wiechert, in *Excitations in Two-Dimensional and Three-Dimensional Quantum Fluids*, edited by A.G.F. Wyatt and H. J. Lauter (Plenum, New York, 1991).
⁷M. Nielsen, J.P. McTague, and W. Ellenson, *J. Phys. C* **38**, C4-10 (1977).
⁸M. Nielsen, J.P. McTague, and L. Passell, in *Phase Transitions in Surface Films*, edited by J.G. Dash and J. Ruvalds (Plenum, New York, 1980).
⁹H. Freimuth, H. Wiechert, and H.J. Lauter, *Surf. Sci.* **189&190**, 548 (1987).
¹⁰H.J. Lauter, V.L.P. Frank, P. Leiderer, and H. Wiechert, *Physica B* **156&157**, 280 (1989).
¹¹H. Freimuth, H. Wiechert, H.P. Schildberg, and H.J. Lauter, *Phys. Rev. B* **42**, 587 (1990).
¹²H.J. Lauter, H. Godfrin, V.L.P. Frank, and P. Leiderer, in *Phase Transitions in Surface Films 2*, edited by H. Taub, G. Torzo, H.J. Lauter, and S.C. Fain, Jr. (Plenum, New York, 1990).
¹³H.J. Lauter, H.P. Schildberg, H. Godfrin, H. Wiechert, and R. Haensel, *Can. J. Phys.* **65**, 1435 (1987).
¹⁴H. Freimuth and H. Wiechert, *Surf. Sci.* **178**, 716 (1986).
¹⁵V.L.P. Frank, H.J. Lauter, and P. Leiderer, *Jpn. J. Appl. Phys., Part 1* **26**, 347 (1987).
¹⁶H.P. Schildberg, H.J. Lauter, H. Freimuth, H. Wiechert, and R. Haensel, *Jpn. J. Appl. Phys., Part 1* **26**, 343 (1987).
¹⁷H.P. Schildberg, H.J. Lauter, H. Freimuth, H. Wiechert, and R. Haensel, *Jpn. J. Appl. Phys., Part 1* **26**, 345 (1987).
¹⁸H. Wiechert, H. Freimuth, H.P. Schildberg, and H.J. Lauter, *Jpn. J. Appl. Phys., Part 1* **26**, 351 (1987).
¹⁹P.R. Kubik, W.N. Hardy, and H. Glattli, *Can. J. Phys.* **63**, 605 (1985).

- ²⁰J.L. Seguin and J. Suzanne, Surf. Sci. **118**, L241 (1982).
²¹J. Chi and S.C. Fain, Jr., Phys. Rev. B **39**, 8628 (1989).
²²M.P.M. den Nijs, J. Phys. A **12**, 1857 (1979).
²³R.J. Baxter, J. Phys. A **13**, L61 (1980).
²⁴B. Nienhuis, J. Phys. A **15**, 199 (1982).
²⁵R.E. Ecke, Q.-S. Shu, T.S. Sullivan, and O.E. Vilches, Phys. Rev. B **31**, 448 (1985).
²⁶M. Bretz, Phys. Rev. Lett. **38**, 501 (1977).
²⁷S. Alexander, Phys. Lett. **54A**, 353 (1975).
²⁸X.-Z. Ni and L.W. Bruch, Phys. Rev. B **33**, 4584 (1986).
²⁹J.M. Gottlieb and L.W. Bruch, Phys. Rev. B **40**, 148 (1989).
³⁰J.M. Gottlieb and L.W. Bruch, Phys. Rev. B **41**, 7195 (1990).
³¹A.D. Novaco, Phys. Rev. Lett. **60**, 2058 (1988).
³²D.M. Ceperley, Rev. Mod. Phys. **67**, 279 (1995).
³³M. Pierce and E. Manousakis, Phys. Rev. B **59**, 3802 (1999).
³⁴M. Pierce, Ph. D Dissertation, Florida State University, 1999.
³⁵P. Sindzingre, D.M. Ceperley, and M.L. Klein, Phys. Rev. Lett. **67**, 1871 (1991).
³⁶D. Scharf, M.L. Klein, and G.J. Martyna, J. Chem. Phys. **97**, 3590 (1992).
³⁷D. Scharf, G.J. Martyna, and M.L. Klein, J. Low Temp. Phys. **19**, 364 (1993).
³⁸M. Wagner and D.M. Ceperley, J. Low Temp. Phys. **94**, 161 (1994).
³⁹M.C. Gordillo and D.M. Ceperley, Phys. Rev. Lett. **79**, 3010 (1997).
⁴⁰M. Wagner and D.M. Ceperley, J. Low Temp. Phys. **102**, 275 (1996).
⁴¹I.F. Silvera and V.V. Goldman, J. Chem. Phys. **69**, 4209 (1978).
⁴²I.F. Silvera, Rev. Mod. Phys. **52**, 393 (1980).
⁴³A.D. Crowell and J.S. Brown, Surf. Sci. **123**, 296 (1982).
⁴⁴W.A. Steele, Surf. Sci. **36**, 317 (1973).
⁴⁵W.E. Carlos and M.W. Cole, Surf. Sci. **91**, 339 (1980).
⁴⁶P.A. Whitlock, G.V. Chester, and B. Krishnamachari, Phys. Rev. B **58**, 8704 (1998).
⁴⁷M. Pierce and E. Manousakis, Phys. Rev. B **62**, 5228 (2000).
⁴⁸M.C. Gordillo and D.M. Ceperley, Phys. Rev. B **58**, 6447 (1998).
⁴⁹M. Pierce and E. Manousakis, Phys. Rev. Lett. **83**, 5314 (1999).
⁵⁰L.W. Bruch, in *Phase Transitions in Surface Films 2*, edited by H. Taub, G. Torzo, H.J. Lauter, and S.C. Fain, Jr. (Plenum, New York, 1990).
⁵¹L. Mattered, C.S. Rosatelli, F. Tommasini, U. Valbusa, and G. Vidali, Surf. Sci. **93**, 515 (1980).